Relationships between Doppler Spectral Moments within Large-Scale Cirro- and Altostratus Cloud Fields Observed by a Ground-Based 95-GHz Cloud Radar

O. DANNE, M. QUANTE, D. MILFERSTÄDT, H. LEMKE, AND E. RASCHKE

Institute for Atmospheric Physics, GKSS Research Centre, Geesthacht, Germany

(Manuscript received 15 September 1997, in final form 2 April 1998)

ABSTRACT

In this study, data obtained from measurements with a ground-based vertical-pointing 95-GHz polarimetric cloud radar are analyzed. The investigations concentrate on the relationships between the Doppler spectral moments observed in different regions of nonprecipitating cirrostratus and altostratus decks connected with warm fronts approaching the radar site. In some of these cases, a remarkably well-defined relationship between the radar reflectivity and the spectral width is found. It is demonstrated how this relationship can be used to obtain information on the size distributions and the fallspeeds of the particles in the investigated cloud sections. It is found that if single parameters of the size distributions, for example, are parameterized by a lognormal distribution, they cannot be determined with an acceptable accuracy. However, at least the changes of these parameters, such as mean particle diameter and particle concentration, with changing reflectivity as well as the behavior of the corresponding particle fallspeeds, can be described with the help of empirical relations between the Doppler moments. A main result is that significant changes in reflectivity within a cloud section (e.g., of 10 dBZ_e) must correspond with a change in the relation between particle size and fallspeed, most commonly described by empirical power laws, and, therefore, probably with changes in particle shapes. This kind of radar data analysis will help to come to a better understanding of the microphysical and dynamical properties of the investigated cloud types, especially if further information from simultaneous measurements with other remote sensors is available.

1. Introduction

Clouds are well known to play a complex and dominant role within the earth's climate system. They modulate the radiation and energy budget and are an important component of the hydrological cycle. Currently, the representation of clouds in general circulation models still appears to be rather poor (Cess et al. 1996). An improved knowledge of the three-dimensional large-scale distribution as well as of the cloud properties on smaller scales is therefore of great importance for the improvement of parameterization schemes for global and regional models. This requires not only long-term observational data for statistical investigations of clouds but also detailed process-oriented studies concerning the microphysical, dynamical, and radiative properties within major systems of specified cloud types.

In recent years, improvements in microwave technology have allowed the development of radars operating at millimeter wavelengths (Lhermitte 1987, 1988). These radars have proven to be an invaluable tool for studying the vertical distribution and the internal structure of, for example, stratiform clouds (e.g., Pazmany et al. 1994; Clothiaux et al. 1995; Syrett et al. 1995; Danne et al. 1996; Kropfli and Kelly 1996). In the fall of 1995, a polarimetric cloud radar (3-mm wavelength) began operation at GKSS Research Centre, Geesthacht, Germany. Until now, this radar has been used for case studies of different stratiform, nonprecipitating cloud systems, for example, stratus decks in winter and cirro- and altostratus layers connected with frontal systems. The data products of the radar include the first three moments of the Doppler spectrum (total power, mean velocity, velocity variance) and polarimetric quantities [Z_{DR}, linear depolarization ratio (LDR)]. As an alternative to the Doppler spectral moments only, full Doppler spectra can also be measured.

This study concentrates on the comparison of the relationships between the Doppler spectral moments within nonprecipitating cirro- and altostratus decks connected with approaching warm fronts. The goal of this kind of analysis is to retrieve information on the underlying particle size distributions and the particle fallspeeds. This is not only a problem because the movement of the particle is always superposed on the un-

Corresponding author address: Dr. Olaf Danne, Institute for Atmospheric Physics, GKSS Research Centre, Max-Planck-Str., 21502 Geesthacht, Germany.
E-mail: danne@gkss.de

derlying wind field but also because of the great variety of the size distributions even on small temporal and spatial scales, which has often been found from in situ measurements with imaging particle probes. If the size distributions are approximated by a lognormal or gamma distribution with three parameters, the relations between the Doppler moments are highly nonlinear and do not allow a straightforward derivation of these parameters with a sufficient accuracy. However, in some of the analyzed cases a remarkably well-defined relationship between the radar reflectivity and the spectral width is found. It is demonstrated how such empirical relationships can be used to obtain information on the underlying particle size distributions and the fallspeeds of the cloud particles. This leads to a better description of the variation of these parameters, such as mean particle diameter and particle concentration with changing reflectivity as well as of the behavior of the corresponding particle fallspeeds. This procedure is applied for selected cloud situations. Furthermore, the results are briefly discussed with regard to the underlying large-scale atmospheric conditions found from radiosonde ascents in the area surrounding the radar site.

2. Underlying theory

In the following section, we describe how empirical relationships between the Doppler spectral moments can be used to obtain information on the cloud particle size distributions (i.e., particle effective diameter, number concentration) in the considered cloud region and on the relations between particle size and fallspeed.

As a starting point, we assume that the size distributions can be sufficiently well described by a distribution with three parameters, which is regarded as a reasonable approach for cirrus clouds (Kosarev and Mazin 1989). Usually, either a lognormal or a modified gamma distribution is applied. In this study, we will use a lognormal distribution, following the notation of Clothiaux et al. (1996):

$$N(D) = \frac{N_t}{\sigma\sqrt{2\pi}D}\exp\left[-\frac{\ln(D/D_n)}{\sigma\sqrt{2}}\right], \quad (1)$$

with the parameters N_t, σ, and D_n. The pth moment of this distribution is given by

$$I_p = \frac{1}{N_t}\int_0^\infty N(D)(D^p\, dD) = D_n^p \exp\left[\frac{1}{2}\sigma^2 p^2\right]. \quad (2)$$

We also assume that the Rayleigh approximation is valid. This is a reasonable approach for the 3-mm radar wavelength considered in this study and nonprecipitating clouds that mainly consist of particles less than a few hundred microns. (Possible errors due to the nonspherical shape of ice particles are mentioned in section 5.)

The radar quantities obtained from the measurements are as follows.

- Reflectivity is expressed as

$$Z_e = \int_0^\infty N(D)(D^6\, dD) = N_t D_n^6 e^{18\sigma^2} = N_t I_6, \quad (3)$$

  where

$$N(D)(D^6) =: S(D) \quad (4)$$

  is the Doppler spectrum.
- For a vertical pointing radar, the Doppler velocity is given by

$$\overline{v} = \frac{\int_0^\infty [v(D) - w(z)]N(D)(D^6\, dD)}{\int_0^\infty N(D)(D^6\, dD)} \quad (5)$$

  with the particle fallspeed v and the vertical wind w, which may be a function of height. For the relation between particle diameter D and fallspeed v we assume, as very common in literature (e.g., Pruppacher and Klett 1978), a power law of the form

$$v(D) = aD^b, \quad (6)$$

  with parameters a and b to be determined. Then (5) becomes

$$\begin{aligned}\overline{v} &= \frac{\int_0^\infty (aD^b - w)N(D)(D^6\, dD)}{\int_0^\infty N(D)(D^6\, dD)} \\ &= \frac{N_t a D_n^{6+b}\exp\left[\frac{\sigma^2}{2}(6+b)^2\right]}{N_t D_n^6 e^{18\sigma^2}} - w \\ &= a\cdot D_n^b \exp\left[6b\sigma^2 + \frac{\sigma^2 b^2}{2}\right] - w. \end{aligned} \quad (7)$$

The vertical wind w can, at least as a first guess, be estimated by taking the average Doppler velocity for all reflectivities lower than a certain threshold (e.g., -30 dBZ_e, negligible fallspeed) in the considered cloud region. In the following, $\overline{v}$ means the measured Doppler velocity at a height z subtracted by $w(z)$. In general, this approach can, of course, be critical because in stratiform clouds the orders of magnitude of vertical winds and particle fallspeeds might be the same. However, for the cloud sections discussed later on we see from the observed Doppler velocities that the particle fallspeeds are obviously large compared to the air motion (large-scale lifting in frontal regions, typically on the order of 0.1 m s^{-1}; low turbulence activity).

For the Doppler width, which we obtain with Eqs. (3), (6), and (7),

FIG. 1. The GKSS 95-GHz polarimetric cloud radar.

TABLE 1. Main characteristics of the GKSS cloud radar.

Frequency (wavelength)	95 GHz (3 mm)
Peak power (EIA)	1.7 kW
Duty cycle	1.2% max
Pulse repetition frequency	50 Hz–80 kHz
Pulse width	50–2000 ns
Beamwidth v_{3dB}	0.17°
Antenna diameter	1.2 m (Cassegrain)
Antenna gain	60 dB
Polarization	Linear (H and V)
Dynamic range	>70 dB

$$\sigma_v^2 = \frac{\int_0^\infty (v(D) - \overline{v})^2 N(D)(D^6\, dD)}{\int_0^\infty N(D)(D^6\, dD)} = a^2 D_n^{2b} e^{12b\sigma^2 + \sigma^2 b^2}[e^{b^2\sigma^2} - 1]. \quad (8)$$

Now consider a time–height region within a cloud with a well-defined $\sigma_v(Z_e)$ relation as often found in the observational data discussed in section 4. It will be seen that this relation can be very well described by an empirical fit of the form

$$\sigma_v = c_1\, \mathrm{dB}Z_e + c_2. \quad (9)$$

With Eqs. (3) and (8), this equation becomes

$$aD_n^b \exp\left[\left(6b + \frac{b^2}{2}\right)\sigma^2\right][e^{b^2\sigma^2} - 1]^{1/2} = 10c_1 \log(N_t D_n^6) + \frac{180 c_1 \sigma^2}{\ln 10} + c_2. \quad (10)$$

Overall, we now have four equations for the five unknowns: a, b, N_t, D_n, and σ. In previous approaches, the relations in Eqs. (3), (7), and (8), together with assumptions for a and b, have been used to derive N_t, D_n, and σ (e.g., Frisch et al. 1995, for water droplets). For ice clouds, this is quite a problem since existing empirical v–D relations (e.g., Locatelli and Hobbs 1974; Mitchell 1996; Pruppacher and Klett 1978) show a wide range of the values for a and b, that is, a varies over two orders of magnitude. This might suggest the strategy to assume a reasonable value for one of the unknowns (or get it from an independent measurement) and then to solve the four equations for the remaining four variables. However, the set of Eqs. (3), (7), (8), and (10), is highly nonlinear, and from a simple error consideration we see for a pair of (Z_e, σ_v) values we also need to know the corresponding value for $\overline{v}$ for the considered cloud section rather exactly to be able to use (7). But from the examples later on we will see that for the same reflectivity value there is often a scatter up to of 2 in the observed Doppler velocities. For example, if we had a standard deviation of a factor of 2 for the Doppler velocity for a given reflectivity value in the cloud section and if $b = 0.5$ (Mitchell 1996), the uncertainty of D_n calculated from Eq. (7) would increase to a factor of 4 even if all other values were known exactly. Only σ can be calculated easily and sufficiently reliably from Eqs. (8) and (7). Division of Eqs. (8) by (7) squared leads to

$$\sigma = \frac{1}{b}\sqrt{\ln\left(1 + \frac{\sigma_v^2}{\overline{v}^2}\right)}. \quad (11)$$

Note that, in contrast to the uncertainty of D_n mentioned above, the error of σ derived in Eq. (11) due to the uncertainty of $\overline{v}$ is much smaller because of the $\sqrt{\ln \ldots}$ term and because the nonlinear terms in Eq. (7) vanish.

Therefore, the idea is now not to calculate absolute values for D_n, N_t, a, and b but to describe separately their changes with changing reflectivity, giving information about the behavior of size distributions and fall velocity laws within a cloud section.

For a given reflectivity, we first calculate the corresponding Doppler width from Eq. (9) and σ from Eq. (11). For $\overline{v}$, which is needed in Eq. (11), we also calculate an empirical fit of the form

$$\overline{v} = c_3\, \mathrm{dB}Z_e + c_4. \quad (12)$$

From Eq. (8) we obtain D_n as a function of a, b, and σ:

$$D_n = \left(\frac{\sigma_v}{a \exp\left[6b\sigma^2 + \frac{\sigma^2 b^2}{2}\right][e^{b^2\sigma^2} - 1]^{-1/2}}\right)^{1/b}. \quad (13)$$

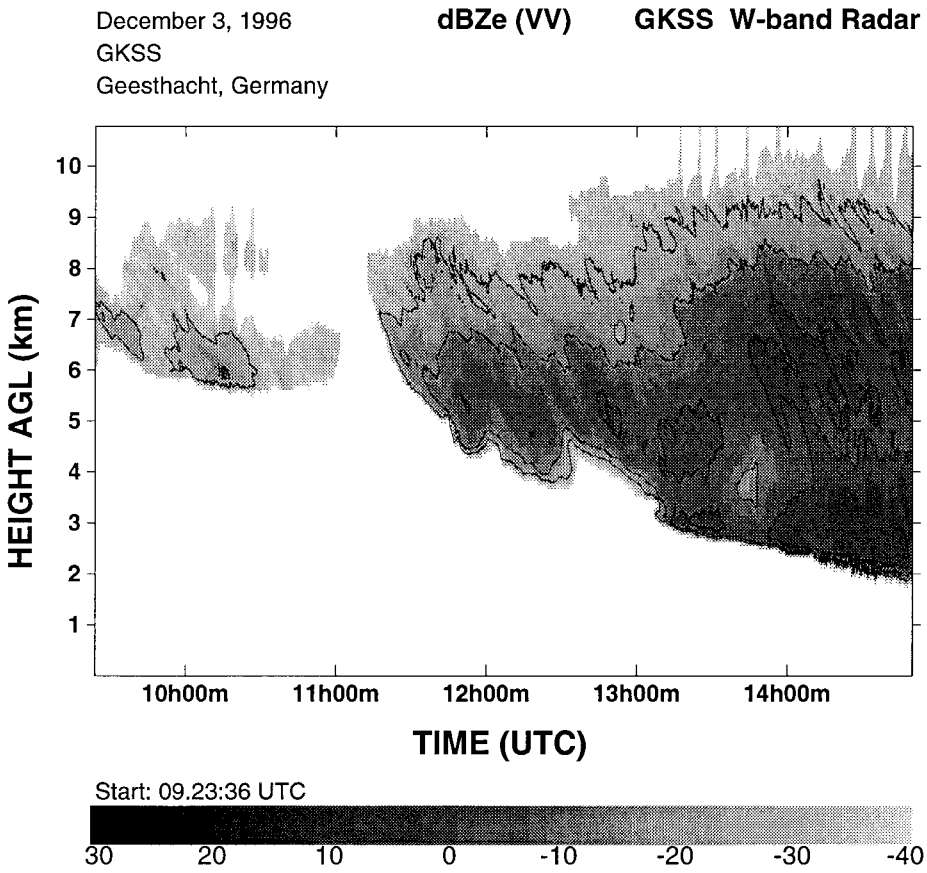

FIG. 2. Height–time section of the radar reflectivity (V polarization, copolar signal) measured with the vertical-pointing GKSS cloud radar on 3 December 1996. The vertical resolution is 75 m; the temporal resolution is 8 s. Contour lines indicate 0, −10, and −20 dBZ_e.

A more commonly used quantity is the particle effective diameter (Hansen and Travis 1974), as defined by

$$D_e = \frac{\int_0^\infty N(D)(D^3\, dD)}{\int_0^\infty N(D)(D^2\, dD)} = \frac{I_3}{I_2} = D_n e^{(5/2)\sigma^2}, \quad (14)$$

and therefore given by

$$D_e = \left(\frac{\sigma_v}{a \exp\left[\frac{7}{2} b\sigma^2 + \frac{\sigma^2 b^2}{2}\right]} [e^{b^2\sigma^2} - 1]^{-1/2} \right)^{1/b}. \quad (15)$$

Finally, N_t can be calculated from Eq. (3):

$$N_t = \frac{Z_e}{D_e^6 e^{3\sigma^2}}. \quad (16)$$

Consequently, we have now the following dependencies between the physical quantities N_t, D_e, σ, a, and b for a given reflectivity and corresponding Doppler width given by c_1 and c_2:

$$\sigma = f_1(b),$$

$$D_e = f_2(a, b, \sigma),$$

and

$$N_t = f_3(D_e, \sigma). \quad (17)$$

For a given range of reflectivities and values for a and b, the quantities σ, D_e, and N_t will be calculated in section 4 for selected cloud situations observed by the radar.

3. The GKSS cloud radar

a. Radar characteristics

In the fall of 1995, a 95-GHz polarimetric cloud radar began operation at GKSS Research Centre, Geesthacht, Germany (Fig. 1). Its main characteristics are listed in Table 1. The number and location of range gates, the pulse repetition frequency, and the pulse length are software selectable. The possible pulse lengths allow for a range resolution between 15 and 300 m. The antenna beamwidth leads to a range cell diameter of about 30 m at 10-km altitude.

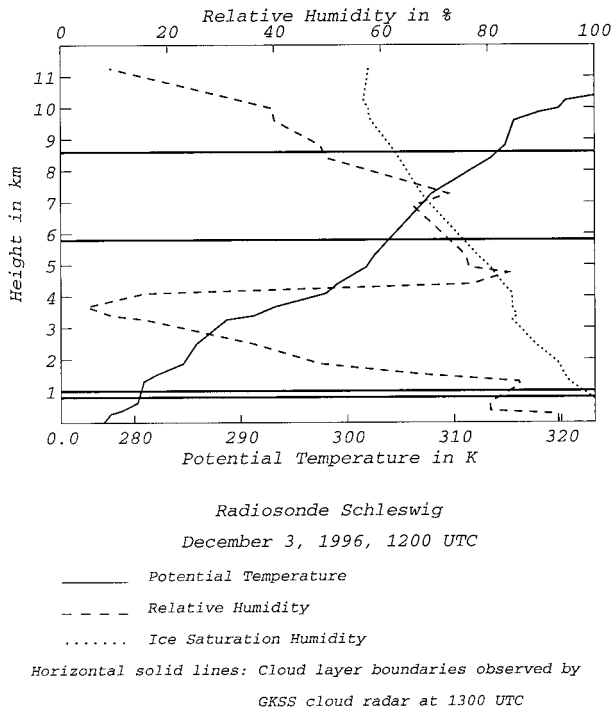

FIG. 3. Vertical profiles of potential temperature and relative humidity obtained from the radiosonde ascent of Schleswig, Germany, 1200 UTC 3 December 1996. For comparison, the horizontal solid and dashed lines mark the cloud-layer top and bottom, respectively, as seen by the GKSS radar at 1300 UTC.

The radar was designed and built by Quadrant Engineering, Inc., Amherst, Massachusetts. The system has been internally calibrated and also operated simultaneously with the externally calibrated Cloud Profiling Radar System (Sekelsky and McIntosh 1996) at Amherst, so the absolute error of the derived reflectivities is probably less than ± 3 dBZ$_e$. This value was confirmed by recent comparisons with in situ forward scattering spectrometer probe data obtained from simultaneous measurements in pure water clouds. The sensitivity of the radar is approximately -30 dBZ at 10-km altitude.

The power source of the system is an extended interaction amplifier. The data processing is based on a Hewlett-Packard VXI data acquisition and processing system. The radar is integrated in an orbit azimuth–elevation scanning system installed in a transportable container for the purpose of ground-based measurements. Until now, the radar has been used for detailed case studies of non- or only light-precipitating stratiform cloud systems.

b. Data products and data processing

The basic data products of the radar are the first three moments of the Doppler spectrum calculated by a pulse-pair algorithm (e.g., Doviak and Zrnić 1993): total power, mean Doppler velocity, and velocity variance. The system is fully polarimetric with horizontal (H) and vertical (V) orthogonal linear polarization directions. From the radar reflecitvities obtained from the received powers in the copolarized and cross-polarized channel, polarimetric quantities such as the LDR and the differential reflectivity (Z_{DR}) can be calculated. Instead of the Doppler moments only, full Doppler spectra can be measured with a 64-point FFT algorithm, but it is not possible at the moment to use the pulse-pair mode and the spectral mode simultaneously.

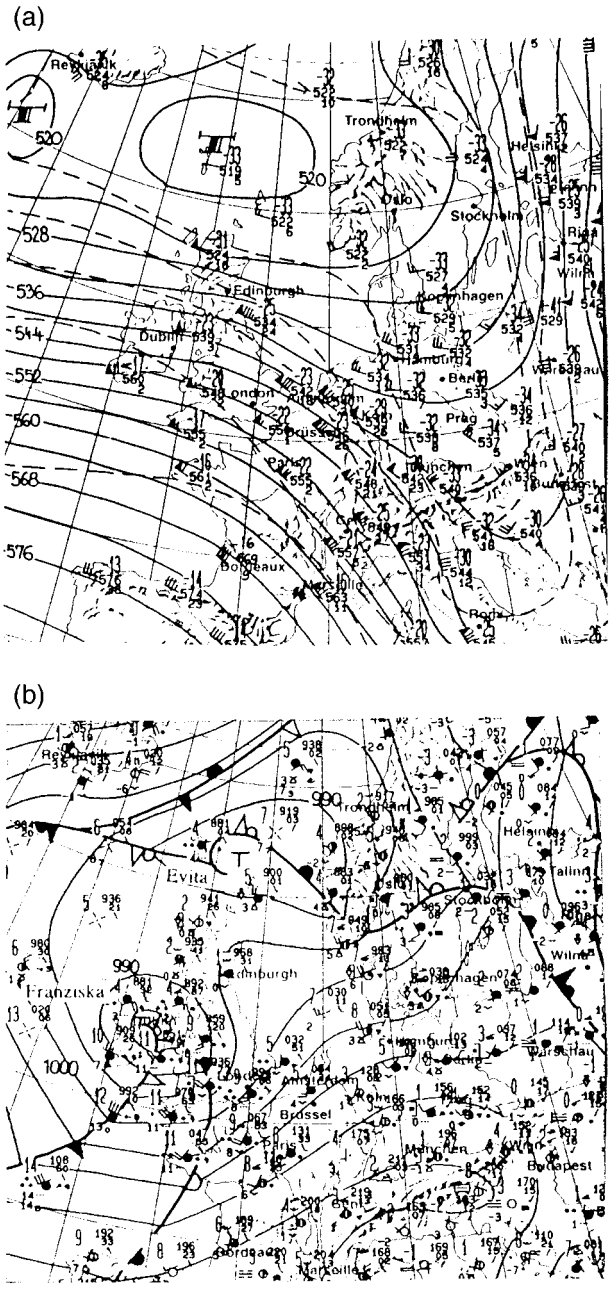

FIG. 4. The 500-hPa and surface analysis for Europe from 0000 UTC 3 December 1996. (Berlin weather map.)

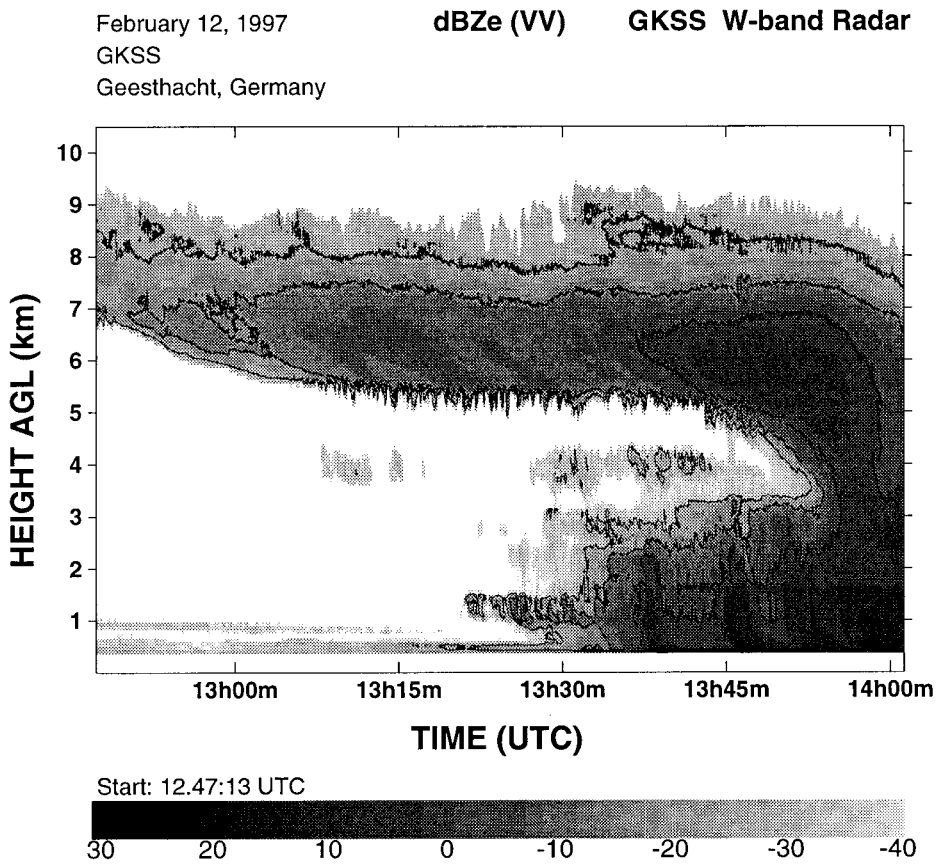

FIG. 5. Height–time section of the radar reflectivity (V polarization, copolar signal) measured with the vertical-pointing GKSS cloud radar on 12 February 1997. The vertical resolution is 75 m; the temporal resolution is 8 s. Contour lines indicate 0, −10, and −20 dBZ$_e$.

Typical height–time sections of radar reflectivities as shown in section 4 are produced in several steps. At first, profiles of received power are calculated by averaging over a large number of samples (in general several thousand pulses). To obtain an estimate for the receiver noise, the 20 contiguous range gates with the lowest average power value in cloud-free regions are determined for each profile. This value is defined as noise power P_n. Initially, a range gate is then set as ''cloudy'' if

$$P \geq P_n + \alpha \frac{1.28(P_n)}{\sqrt{M}}, \tag{18}$$

where P is the signal-plus-noise power and M is the number of samples (Marshall and Hitschfeld 1953). The factor 1.28 appears from the logarithmic form of the receiver transfer function. However, the value of α can be adjusted and is somewhat arbitrary (Clothiaux et al. 1995). For the data presented in section 4, a value of $\alpha = 2$ was used. In the next step, a binary cloud mask is applied to remove the remaining speckle noise in cloud-free regions. This procedure, applied for both H and V received powers, is described in detail by Clothiaux et al. (1995). For the remaining cloudy range gates, the corresponding H and V radar reflectivities are calculated from the radar equation. The pulse-pair estimates of mean Doppler velocity and spectral width are also determined for these gates. For each gate, the noise power P_n as calculated above is subtracted from the zero lag autocovariance term, following Doviak and Zrnić (1993). Note that this method only removes the white noise contribution from the receiver; therefore, noise in backscatter or radar phase noise may still be present and can bias the spectral widths in low signal-to-noise conditions (Lhermitte 1987). However, only data based on relatively high signal-to-noise ratios (SNRs) are discussed in this study. Random uncertainties in the pulse-pair estimates, which are also a function of SNR and of signal dwell time, will be discussed in section 5 with regard to the present data.

4. Measurements and results

In this section, the ideas outlined in section 2 will be applied to selected situations with large-scale cirro- and altostratus cloud fields connected with warm fronts approaching the radar site.

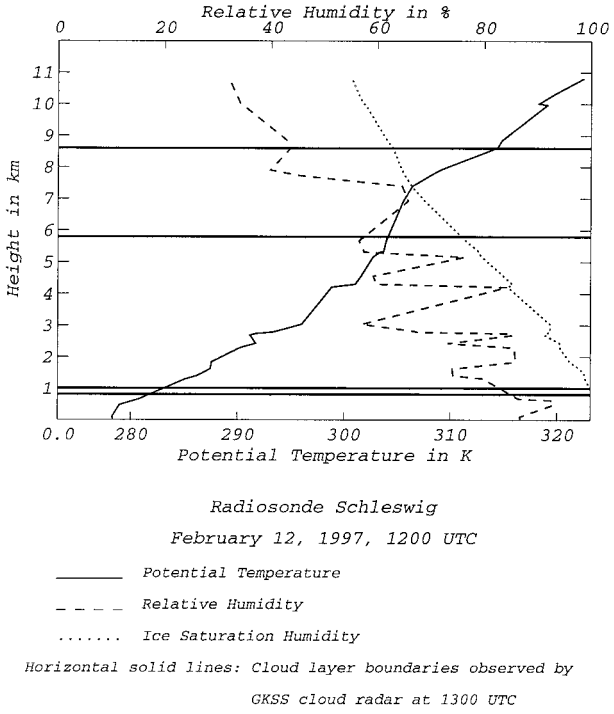

FIG. 6. Vertical profiles of potential temperature and relative humidity obtained from the radiosonde ascent of Schleswig, Germany, 1200 UTC 12 February 1997. For comparison, the horizontal solid and dashed lines mark the cloud-layer tops and bottoms, respectively, as seen by the GKSS radar at 1300 UTC.

a. Synoptic description of the cloud situations

The first cloud field considered here was observed by the GKSS cloud radar on 3 December 1996, at Geesthacht, which is located in northern Germany about 40 km southeast of Hamburg. Figure 2 shows a height–time section of the radar reflectivity (vertical-pointing radar) for a period of about 5 h. The reflectivities were calculated from the copolarized signal (vertical polarization transmitted and received) and are given in dBZ_e. This typical frontal cirro- and altostratus deepened more and more and later changed into a nimbostratus. At about 1500 UTC, moderate rainfall started so that the radar operation was stopped. In this cloud, the reflectivity increases with decreasing height, indicating the presence of generally larger particles in the lower cloud region. Another remarkable feature is the very inhomogeneous cloud base after 1400 UTC. For the observer at the ground, this cloud base appeared as small-scale, mammatus-like structures, indicating precipitation that falls out of the cloud and quickly evaporates in an environment with much lower humidity. This is confirmed by the large-scale atmospheric conditions found from the radiosonde ascent at Schleswig from 1200 UTC (Fig. 3). Schleswig is located about 100 km north of the GKSS radar site, but almost parallel to the approaching front axis; therefore, this radiosonde ascent is the best suited in the surrounding area for comparison with the

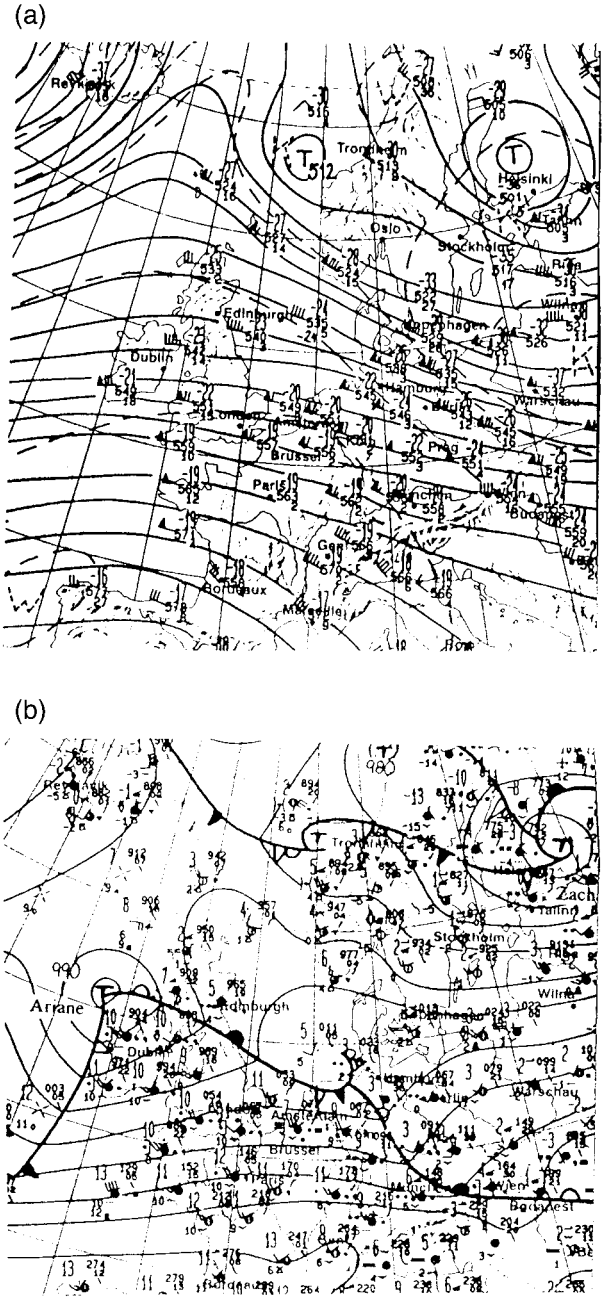

FIG. 7. The 500-hPa and surface analysis for Europe from 0000 UTC 12 February 1997. (Berlin weather map.)

radar data. The humidity profile corresponds very well with the cloud boundaries observed by the radar, and a very sharp decrease of humidity can be seen below 4 km. This result illustrates the link between small-scale cloud features and the underlying atmospheric conditions on much larger scales. The large-scale flow pattern in the height region of the cloud field (e.g., 500 hPa at 0000 UTC, Fig. 4a) clearly shows the advection of warm air on the backside of a deep trough over eastern Europe. The corresponding surface map (Fig. 4b) shows a storm

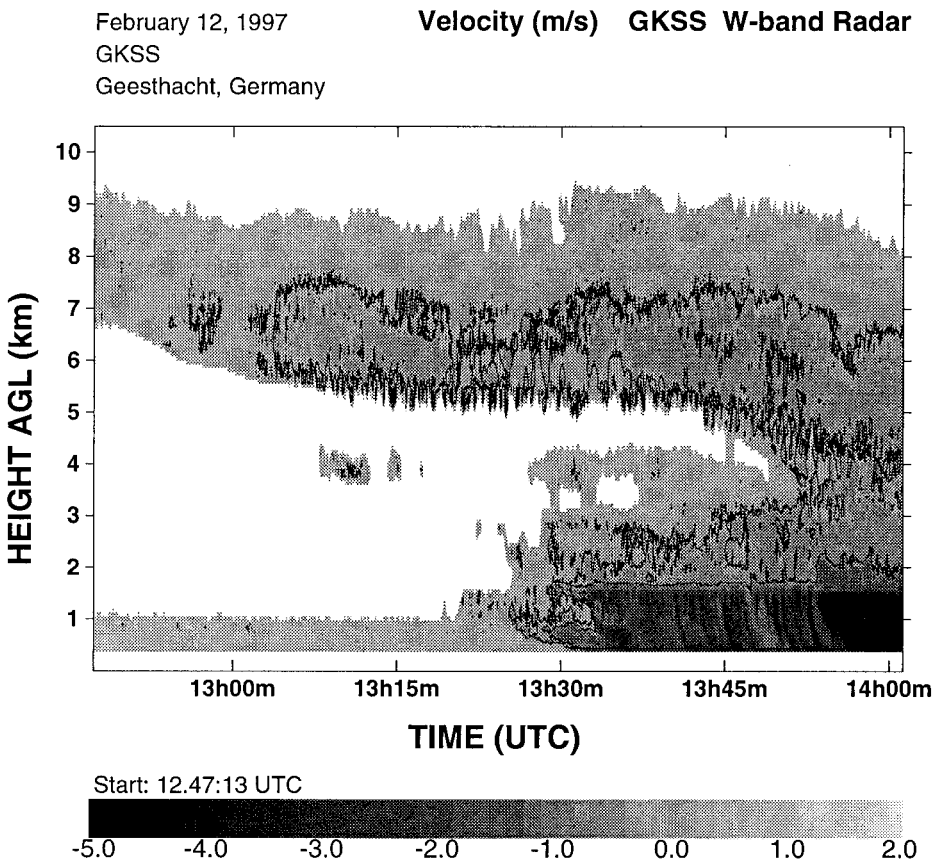

FIG. 8. Height–time section of the Doppler velocity measured with the vertical-pointing GKSS cloud radar on 12 February 1997. Negative values indicate downward motion. The vertical resolution is 75 m; the temporal resolution is 8 s. Contour lines indicate -0.5 and -1.0 m s^{-1}.

over Ireland moving eastward. The warm front passed the radar site from west to east at about 1800 UTC.

The second cloud situation was observed on 12 February 1997. Figure 5 shows a height–time section of the radar reflectivity (copolar signal) from 1247–1400 UTC. At the beginning, we also see cirro- and altostratus that slightly thickens with time, but after 1330 UTC, a compact nimbostratus cloud quickly reached the radar site. Rainfall started at about 1355 UTC, indicated by fallstreaks and a well-developed bright band at about 1.7-km altitude. For the observer on the ground, this cloud system was hidden by a shallow, but optically thick stratus layer below 1-km altitude. The corresponding atmospheric conditions are shown in Fig. 6 (radiosonde ascent of Schleswig at 1200 UTC) and Fig. 7 (500 hPa and surface maps at 0000 UTC). In this case, the humidity is relatively high throughout most parts of the troposphere, which may explain the fast approach of the nimbostratus cloud over the radar site. The flow pattern in 500 hPa looks similar to the 3 December case, but it is generally more zonal. The surface map also shows a storm west of Ireland that deepened and moved eastward. The wavelike depression along the warm front moved southeastward; the cloud system observed by the radar belonged to the part of the front closer to the center of the storm. This front moved in a more eastward direction.

b. Relationships between the Doppler moments

The moments of the Doppler spectrum introduced in section 2 will now be analyzed in more detail, that is, the relationships among radar reflectivity, Eq. (3); Doppler velocity, Eq. (7); and Doppler width, Eq. (8). As an example for the velocities and widths corresponding to the reflectivities shown in section 4a, Figs. 8 and 9 show the Doppler velocity and the Doppler width, respectively, for the height–time region in Fig. 5. The highest fall velocities occur below the melting layer, which is consistent with the presence of liquid, spherical particles that have much higher terminal velocities than ice crystals or snowflakes. The patterns of reflectivity and Doppler width obviously show a correlation between low widths and high reflectivities in the cloud region above the melting layer. On the other hand, the spectral widths show a sharp increase in the melting layer region, which is not obvious in the reflectivity pattern. This leads to the conclusion that the Doppler

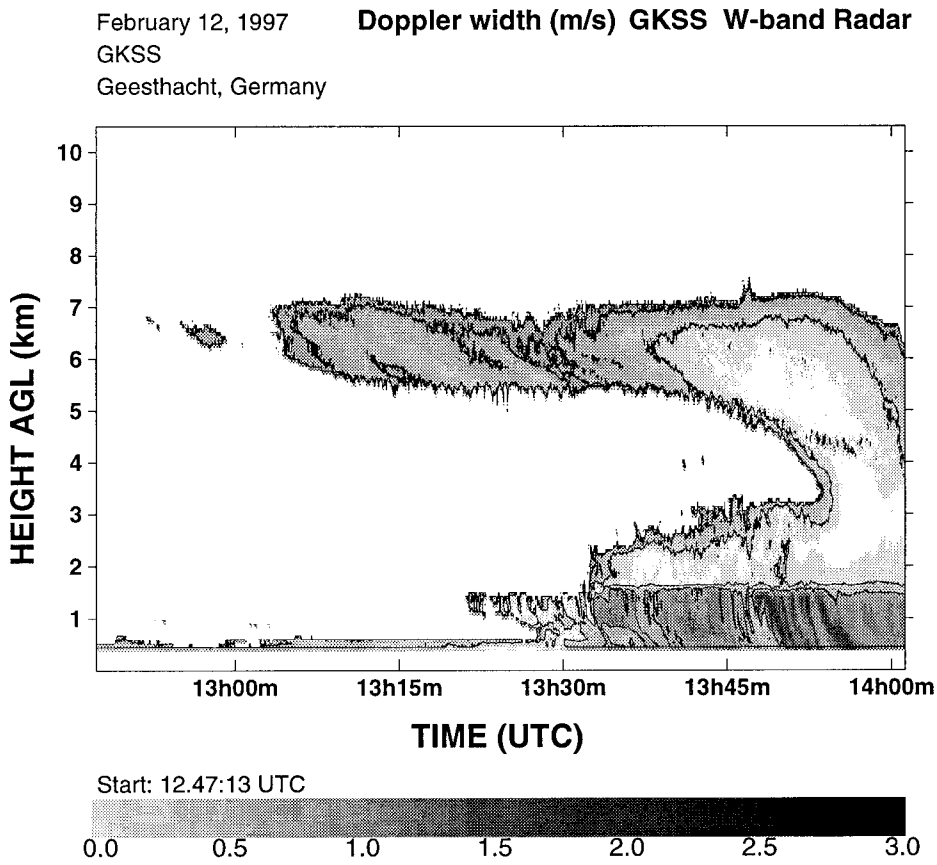

FIG 9. Height–time section of the Doppler width measured with the vertical-pointing GKSS cloud radar on 12 February 1997. The vertical resolution is 75 m; the temporal resolution is 8 s. Contour lines indicate 0.3, 0.6, and 0.9 m s^{-1}. Only spectral widths with SNR $> +5$ dB are shown.

widths above the melting layer are determined more by the population of the particles than by turbulence activity on scales smaller than the radar resolution volume that would correspond to a wider range of widths within regions of about the same reflectivity. In this cloud region, an increase of the reflectivity seems to be caused by an increase of particles of one typical size, which then results in a narrowing of the peak in the Doppler spectrum, thereby explaining the lower spectral width. On the other hand, the enhanced spectral widths below the bright band are probably caused by a superposition of cloud droplets and larger raindrops that will likely result in multimodal Doppler spectra.

The behavior of reflectivities and the corresponding spectral widths was investigated in more detail for several height regions within the stratiform cloud systems shown in Figs. 2 and 5. As examples, Figs. 10a,b and 11a,b show reflectivity versus Doppler width and reflectivity versus Doppler velocity, respectively, each for 10 consecutive range gates (vertical resolution of 75 m) within the altostratus regions of these cases. From nearby radiosonde ascents, the temperature was found to be less than -30°C for these altitudes in both cases, therefore it can be assumed that these clouds mainly consist of ice particles. Well-defined relations between reflectivity and width (almost linear if reflectivities are given on a logarithmic scale) can be seen for both cases with correlation coefficients $|r| > 0.9$ for a linear regression. To give an impression of the underlying SNRs, the reflectivity with SNR $= +5$ dB at a height of 6000 m is marked by dashed lines.

Since these correlations are remarkably high, the question is raised whether the pulse-pair estimates of the spectral widths might be artificially biased by remaining noise that could not be removed by Eq. (18). We do not think so. The main reason is that the empirical relations in Figs. 10a and 11a are valid up to reflectivities of more than $+5$ dBZ_e, which corresponds to a rather high SNR of more than $+20$ dB. The range of values of the spectral widths agrees well with results previously published by Lhermitte (1987), who discussed a similar type of cloud. To confirm that there is no artifact, we investigated the reflectivities and spectral widths from several other stratiform, high- and midlevel cloud systems that were obtained under similar experimental conditions, that is, with the same radar param-

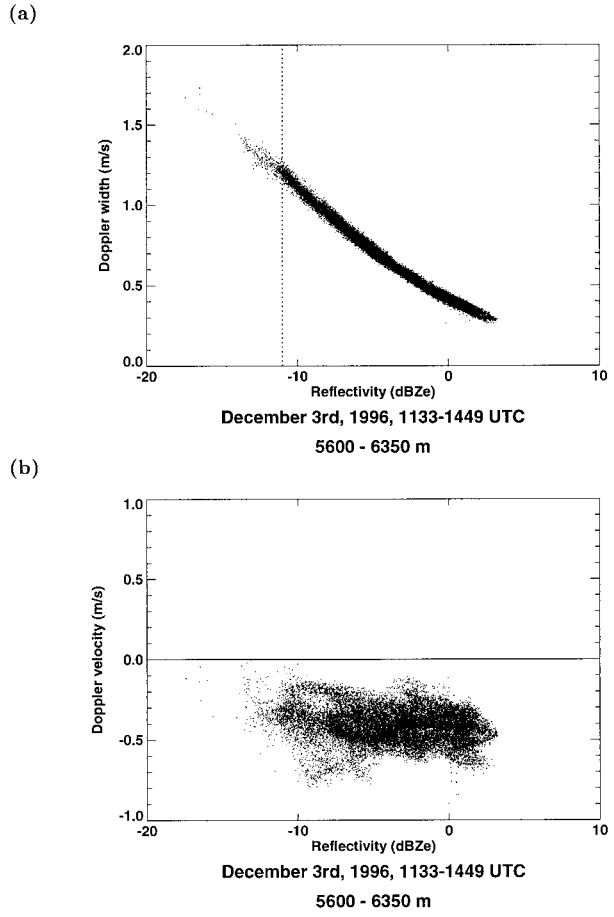

FIG. 10. Scatterplots of (a) reflectivity vs Doppler width and (b) reflectivity vs Doppler velocity for a selected height region of the cloud section shown in Fig. 2. In (a), the reflectivity with corresponding SNR = +5 dB at a height of 6000 m is marked by a dashed line.

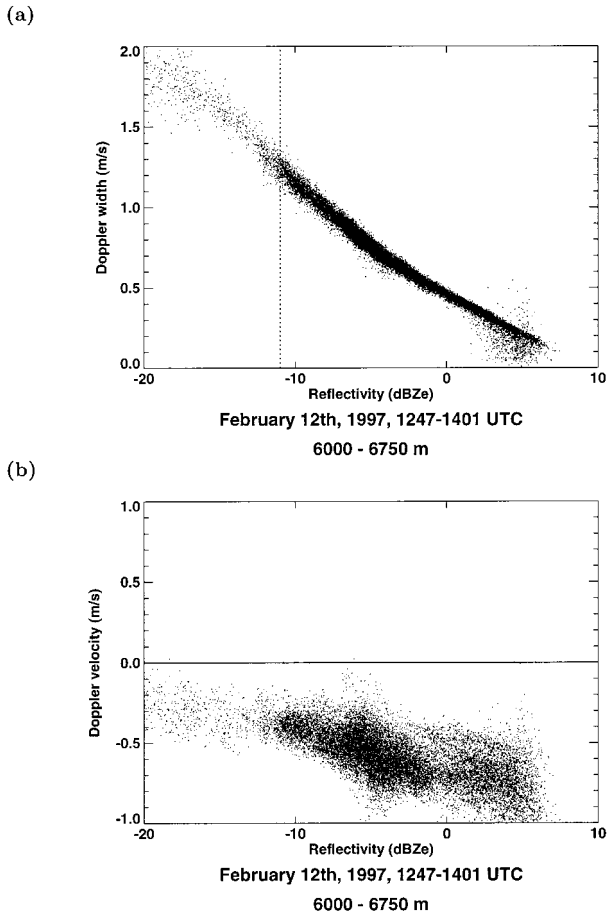

FIG. 11. Scatterplots of (a) reflectivity vs Doppler width and (b) reflectivity vs Doppler velocity for a selected height region of the cloud section shown in Fig. 5. In (a), the reflectivity with corresponding SNR = +5 dB at a height of 6000 m is marked by a dashed line.

eters such as pulse repetition frequency (PRF), pulse length, and number of samples. Two examples are shown in Fig. 12. The correlation in Fig. 12b is much lower than in Figs. 10a and 11a, and in Fig. 12a almost no correlation is found, showing that the procedure for data analysis presented in this study is applicable for specified cloud situations, but not in general.

The relations between reflectivity and velocity are not as obvious ($|r| \sim 0.2$), although a slight increase of fall velocities with increasing reflectivities can be seen. With regard to a regression line calculated from Eq. (12), the standard deviations of the velocities for a given reflectivity are on the order of 0.2 m s^{-1}. These deviations could be explained with fluctuations of the vertical wind on scales larger than the radar resolution volume. For other height bands, similar results were found for both 3 December and 12 February.

For the 12 February case, we now follow the procedure described in section 2 for a more detailed investigation of the properties of the particle size distributions and the particle fall speeds. For all pairs of (Z_e, σ_v) values within the considered cloud section, the values of c_1 and c_2 are calculated from Eq. (9), and the functions f_1, f_2, and f_3 in Eq. (17) are obtained. The values of $\overline{v}$, which are needed in f_1 to determine σ, are calculated from Eq. (12). The parameters σ, D_e, and N_t describing the size distribution are then calculated for a reasonable range of values for a and b. From the several relations given by Pruppacher and Klett (1978) for ice clouds, values of b are found to be in the range between about 0.5 and 1.5, whereas a may vary over two orders of magnitude (~10–1000). As an example, Figs. 13, 14, and 15 show σ, D_e, and N_t, respectively, as a function of the reflectivity in the range from −10 to 0 dBZ_e for $a = 10$ m^{1-b} s^{-1} and b ranging from 0.7 to 1.1. The changes in σ are small for either changes in b or in dBZ_e, whereas the behavior of D_e and N_t needs more discussion. If we assume D_e to be in the range of 10–100 μm and N_t on the order of 0.1 cm^{-3} (as often found from in situ measurements in ice clouds), the observed range of reflectivities in the cloud section must correspond to a significant change of b (decreasing val-

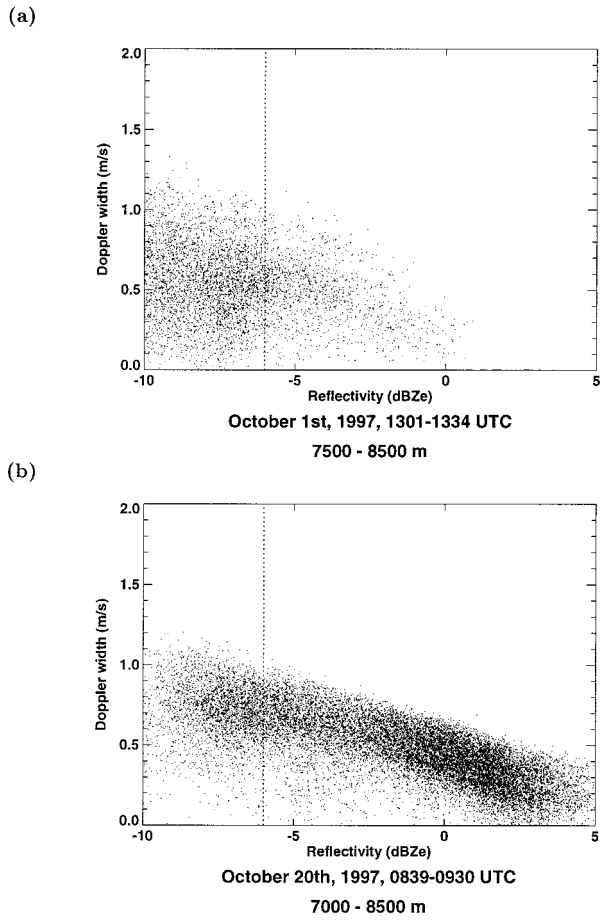

FIG. 12. Scatterplots of reflectivity vs Doppler width for sections of cirrostratus clouds on (a) 1 October and on (b) 20 October. Time and height resolution are 8 s and 75 m, respectively, for both cases. The reflectivity with corresponding SNR = +5 dB at a height of 7500 m is marked by a dashed line.

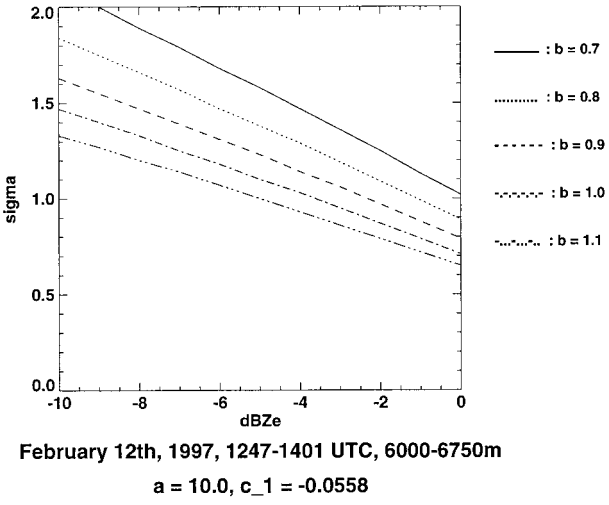

FIG. 13. Size distribution parameter σ as a function of the radar reflectivity for a range of values of b for the same height region as in Figs. 11a,b.

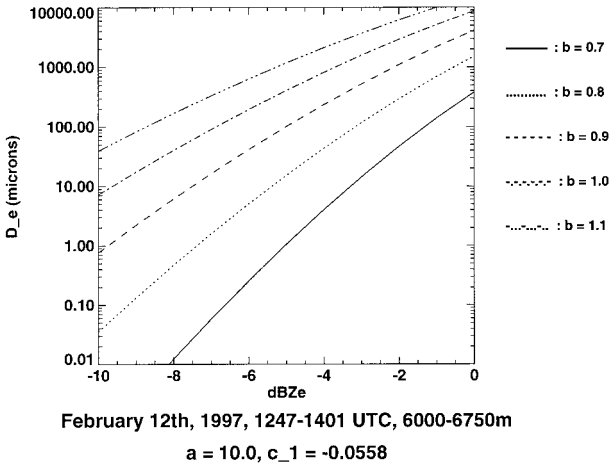

FIG. 14. Same as Fig. 13 but for the effective diameter D_e.

ues of b for increasing reflectivities). On the other hand, the influence of an increase of a is not large; Fig. 16, with $a = 1000$ m^{1-b} s^{-1}, is similar to Fig. 14 with $a = 10$ m^{1-b} s^{-1}. For a (dBZ_e, D_e) pair, the corresponding value of b is shifted by only about 0.1. The same calculations were carried out for the 3 December case with very similar results.

Although not explicitly used for the procedure discussed above, the relation between Doppler velocity and Doppler width was also investigated. Figure 17 shows this relation for 12 February for the same cloud section as above. High widths seem to be related to low fall speeds, but the correlation is rather poor ($r < 0.1$). Similar results were obtained for different height regions and also for the 3 December case. This result again suggests the presence of fluctuations of the vertical wind on scales larger than the radar resolution volume that affect the Doppler velocities, but not the widths.

The findings shown above indicate that for these

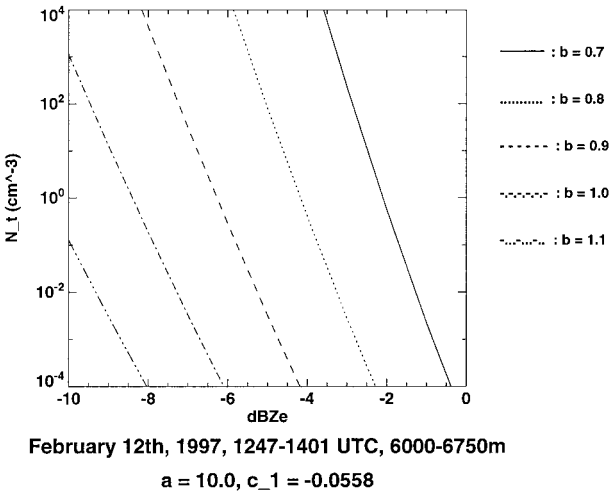

FIG. 15. Same as Fig. 13 but for the particle concentration N_t.

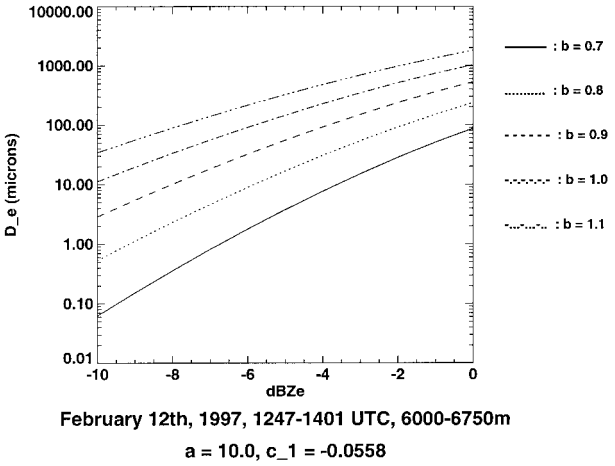

FIG. 16. Same as Fig. 14 but for $a = 1000$.

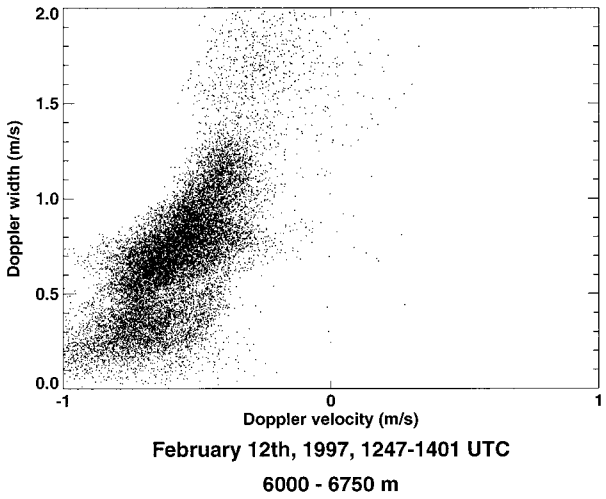

FIG. 17. Scatterplot of Doppler velocity vs Doppler width for the same cloud region as in Fig. 11a.

two cases an increase of radar reflectivities is related to a change of the relation of particle diameter and fall speed. The decreasing values of b show that the increase of the fall speed of the particles with increasing diameter becomes slower, probably due to an increase of the drag coefficient, meaning that the particle shape probably becomes more complex. This guess is confirmed by the corresponding polarimetric data of the cloud radar. Figure 18 shows the LDR, defined as the ratio of the reflectivities calculated from the received powers in the cross- and the copolar channels, respectively, for the same cloud section as shown in Fig. 5. In the cloud region around 6-km altitude, a slight increase of LDR is visible between about 1335 and 1350 UTC, which corresponds to the increase of the copolar reflectivity in this region as seen in Fig. 5. From theoretical scattering calculations it is well known that more complex particle shapes lead to a higher degree of depolarization as observed here.

It is also noted that, even with the support of well-defined Z_e–σ_v relationships as found here, single parameters of a particle size distribution cannot be determined with sufficient accuracy (which is not surprising at all). However, from Fig. 14 to Fig. 16 we see that we can at least derive a range of values for b if reasonable values for N_t and D_e are considered. Once a range of values for b is known, we obtain a quite good estimate for the values of σ. For example, with the assumption of D_e to be within 10 and 100 μm, we have a range of b from about 1.1 to 0.6 in the considered reflectivity range, giving a value of $\sigma \approx 1.3$ from Fig. 13.

5. Error discussion

The derivation of properties of cloud particle size distributions from remote sensing measurements with a single instrument such as a cloud radar has been recognized as a difficult task (e.g., Clothiaux et al. 1996; Frisch et al. 1995; Gossard et al. 1997; Gossard 1994). This is especially true for ice clouds, as considered in this study. The first error source could be the assumption of the validity of the Rayleigh approximation in Eq. (3). This error is probably negligible for particles that have a nearly spherical shape, but it could become significant for more complex particles such as crystal aggregates. Theoretical calculations of the scattering characteristics of these complex-shaped particles have to be carried out to evaluate the validity of the Rayleigh approximation at 3-mm wavelength. Adequate algorithms would be the discrete dipole approximation (Schneider and Stephens 1995) or the conjugate gradient–fast Fourier transform method (Sarkar et al. 1986).

Reflectivities as used in Eq. (3) may also be biased toward too low values due to attenuation by liquid water. However, both investigated cloud systems are located in relatively high altitudes (bases > 3 km for most of the investigated time periods of the two cases), so it can be assumed that both cloud systems mainly consist of ice, which causes only very low attenuation with values comparable to attenuation by atmospheric gases in the cloud-free, low troposphere (Ulaby et al. 1981). Significant attenuation is only visible in the last 5 min of the reflectivity height–time section of 12 February (Fig. 5) when rainfall had started. The reflectivities in about 4–7 km are obviously reduced compared with a few minutes earlier, whereas the light rain causes rather high reflectivities close to the ground. However, exclusion of these 5 min hardly changed the results shown in Fig. 11, therefore effects of attenuation are not further considered here.

Another error source that is always present in Doppler radar measurements is the superposition of particle fall speeds and the air movement due to a nonzero mean vertical and horizontal wind as well as turbulent mo-

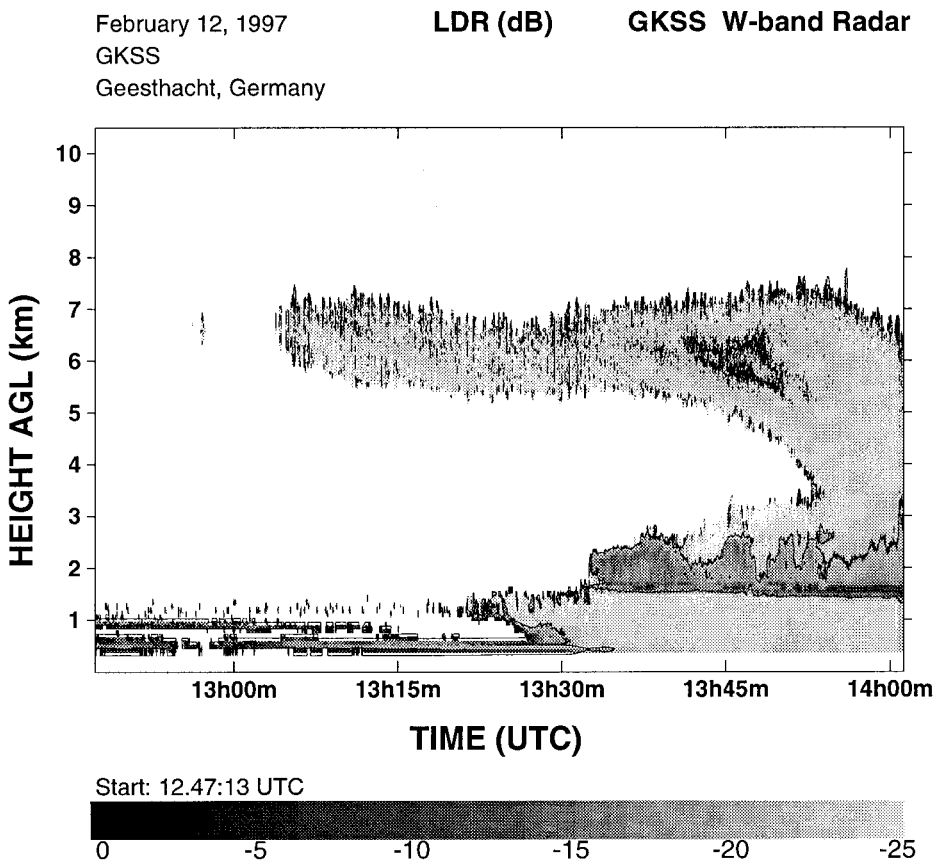

FIG. 18. Height–time section of the linear depolarization ratio (LDR) measured with the vertical-pointing GKSS cloud radar on 12 Feb 1997. Contour lines indicate −10, −15, and −20 dB.

tions. For the investigations shown above, a superposed mean vertical wind is not that important since it is probably small compared to the observed Doppler velocities, and the turbulence intensity on scales within the radar resolution volume was found to also be probably very small. However, turbulent motions on larger scales (e.g., several hundred meters) are difficult to estimate; they obviously appear in the Doppler velocities causing the weak correlation with the reflectivities and with the Doppler widths. We also have to keep in mind that the vertical alignment of the cloud radar must be very exact to suppress contamination by horizontal wind components. For both selected cloud cases, the horizontal wind speed found from the surrounding radiosonde ascents was on the order of 20 m s^{-1} in the selected height regions. A tilt of the radar beam of only 0.3° into the direction of the horizontal wind would then cause a vertical component of about 0.1 m s^{-1}, which may also partly explain the scatter in the observed Doppler velocities.

We also have to mention random errors of the pulse-pair estimates. Both errors of Doppler velocity and spectral width depend on signal dwell time, SNR, and spectral width itself (Doviak and Zrnić 1993). These errors do not significantly influence the results of this study. For example, for SNR = 0 dB, a PRF of 10 kHz and a spectral width of 1 m s^{-1}, the random error is 0.036 m s^{-1} for the Doppler velocity and 0.16 m s^{-1} for the spectral width. These errors decrease for increasing SNR. For example, for SNR = +10 dB, the errors are 0.027 m s^{-1} and 0.006 m s^{-1} for the velocity and the spectral width, respectively.

The pulse-pair estimates of Doppler velocity and Doppler width would also contain errors if different particle populations were present in the radar volume causing multimodal Doppler spectra, that is, if large rain or snow particles fall into a cloud layer consisting of small particles. However, this problem probably does not occur in the cloud sections considered here, except the regions below the melting layer as seen in Fig. 5.

Another error source in the spectral widths under low signal-to-noise conditions could be white noise in backscatter or radar phase noise. This error is difficult to estimate, but, as already pointed out in sections 3 and 4, the results of this study were derived for SNRs that are relatively high.

6. Summary and conclusions

In this study, data obtained from measurements with a ground-based vertical pointing 95-GHz cloud radar

was investigated with regard to the relationships between the Doppler spectral moments observed within cirro- and altostratus clouds connected with warm front passages. Well-defined relationships between the radar reflectivity and the Doppler width were found in the data. Based on this, a procedure was proposed to retrieve information on the underlying particle size distributions and the particle fallspeeds. It was found that the observed changes in reflectivity within a cloud section must correspond to a change in the relation between particle size and fallspeed and therefore probably with changes in particle shapes. With the proposed method it is still not possible to retrieve full particle size distributions that can be described by a lognormal distribution with three parameters, but at least the parameter σ (the width of the distribution) can be determined quite well. In example, it was found to be very uniform (about 1.3) in the reflectivity range between -10 and 0 dBZ_e for the two selected cloud cases. The results also illustrate the relationships between the other two parameters of the distribution: 1) number concentration N_t and particle effective diameter D_e and 2) the parameters describing the relation between particle size and fall speed. Once a good estimate for one of these remaining unknown quantities is available, that is, from an independent measurement, these results will be very helpful in coming closer to a better description of particle size distributions even within ice clouds if well-defined empirical relations between the Doppler moments are found in the data. As shown at the end of section 4, the determination of polarimetric quantities, such as the linear depolarization ratio, can also be very helpful to check assumptions on the particle populations.

For future investigations, the measurements of full Doppler spectra during short time periods within long-term measurements of the Doppler moments as discussed here could also be helpful. First datasets of Doppler spectra have been collected, but one must keep in mind that with the available 64-point FFT algorithm either the frequency resolution is poor or the Nyquist interval (range of unambiguous Doppler frequencies) is rather small. Further investigations are necessary on how the combination of pulse-pair and spectral data processing can be optimized. For more efficient FFT measurements, supplying more memory and a faster processor to the data processing system of the GKSS radar is also planned.

It can finally be concluded that the quantities measured by remote sensing instruments need to be known very exactly to be used as an input for the nonlinear equations that relate the Doppler moments with the parameters of the size distributions. As determined in many previous studies related to cloud radars (e.g., Matrosov et al. 1992; Matrosov 1993; Intrieri et al. 1993), the simultaneous use of several remote sensing instruments working at different wavelengths is desirable in the future to reduce the occurring errors due to inaccuracies in the measured quantities.

Acknowledgments. We wish to thank all the people who were involved in the setup of the GKSS cloud radar and in recording the measurements. We especially thank Dr. Ivan PopStefanija from Quadrant Engineering, Inc., Amherst, Massachusetts, for his presence and for all his help during the intensive test measurements when the radar was set up at the GKSS site. We also would like to thank Dr. Eugene Clothiaux from Pennsylvania State University, Department of Meteorology, for many helpful suggestions concerning the data processing and for fruitful discussions during his stay at GKSS, which was supported by a NATO Collaborative Research Grant. The authors would finally like to thank Prof. Yasushi Fujiyoshi from Hokkaido University, Institute of Low Temperature Science, for many useful comments on the interpretation of cloud radar data and for the collaboration during his 1-yr stay at GKSS.

REFERENCES

Cess, R. D., and Coauthors, 1996: Cloud feedback in atmospheric general circulation models: An update. *J. Geophys. Res.,* **101,** 12 791–12 794.

Clothiaux, E. E., M. A. Miller, B. A. Albrecht, T. P. Ackerman, J. Verlinde, D. M. Babb, R. M. Peters, and W. J. Syrett, 1995: An evaluation of a 94-GHz radar for remote sensing of cloud properties. *J. Atmos. Oceanic Technol.,* **12,** 201–229.

——, T. P. Ackerman, and D. M. Babb, 1996: Ground-based remote sensing of cloud properties using millimeter-wave radar. *Radiation and Water in the Climate System: Remote Measurements,* E. Raschke, Ed., NATO, 323–366.

Danne, O., G. G. Mace, E. E. Clothiaux, X. Dong, T. P. Ackerman, and M. Quante, 1996: Observing structures and vertical motions within stratiform clouds using a vertical pointing 94-GHz cloud radar. *Contrib. Atmos. Phys.,* **69,** 229–237.

Doviak, R. J., and D. S. Zrnić, 1993: *Doppler Radar and Weather Observations.* 2nd Ed. Academic Press, 458 pp.

Frisch, A. S., C. W. Fairall, and J. B. Snider, 1995: Measurement of stratus cloud and drizzle parameters in ASTEX with a K_a-band Doppler radar and a microwave radiometer. *J. Atmos. Sci.,* **52,** 2788–2799.

Gossard, E. E., 1994: Measurement of cloud droplet size spectra by Doppler radar. *J. Atmos. Oceanic Technol.,* **11,** 712–726.

——, J. B. Snider, E. E. Clothiaux, B. Martner, J. S. Gibson, R. A. Kropfli, and A. S. Frisch, 1997: The potential of 8-mm radars for remotely sensing cloud drop size distributions. *J. Atmos. Oceanic Technol.,* **14,** 76–87.

Hansen, J. E., and L. D. Travis, 1974: Light scattering in planetary atmospheres. *Space. Sci. Rev.,* **16,** 527–610.

Intrieri, J. M., G. L. Stephens, W. L. Eberhard, and T. Uttal, 1993: A method for determining cirrus cloud particle sizes using lidar and radar backscatter techniques. *J. Appl. Meteor.,* **32,** 1074–1082.

Kosarev, A. L., and I. P. Mazin, 1989: Empirical model of physical structure of the upper level clouds of the middle latitudes. *Radiation Properties of Cirrus Clouds,* Nauka, 29–52.

Kropfli, R. A., and R. D. Kelly, 1996: Meteorological research applications of mm-wave radar. *Meteor. Atmos. Phys.,* **59,** 105–121.

Lhermitte, R., 1987: A 94-GHz Doppler radar for cloud observations. *J. Atmos. Oceanic Technol.,* **4,** 36–48.

——, 1988: Cloud and precipitation remote sensing at 94 GHz. *IEEE Trans. Geosci. Remote Sens.,* **26,** 207–216.

Locatelli, J. D., and P. V. Hobbs, 1974: Fall speeds and masses of solid precipitation particles. *J. Geophys. Res.,* **79,** 2185–2197.

Marshall, J. S., and W. Hitschfeld, 1953: Interpretation of the fluc-

tuating echo from randomly distributed scatterers. *Can. J. Phys.*, **31,** 962–995.

Matrosov, S. Y., 1993: Possibilities of cirrus particle sizing from dual-frequency radar measurement. *J. Geophys. Res.*, **98,** 20 675–20 683.

——, T. Uttal, J. B. Snider, and R. A. Kropfli, 1992: Estimation of ice cloud parameters from ground-based infrared radiometer and radar measurements. *J. Geophys. Res.*, **97,** 11 567–11 574.

Mitchell, D. L., 1996: Use of mass- and area-dimensional power laws for determining precipitation particle terminal velocities. *J. Atmos. Sci.*, **53,** 1710–1723.

Pazmany, A., J. Mead, R. McIntosh, M. Hervig, R. Kelly, and G. Vali, 1994: 95-GHz polarimetric radar measurements of orographic cap clouds. *J. Atmos. Oceanic Technol.*, **11,** 140–153.

Pruppacher, H. R., and J. D. Klett, 1978: *Microphysics of Clouds and Precipitation.* D. Reidel, 714 pp.

Sarkar, T. K., E. Arvas, and S. M. Rao, 1986: Application of FFT and the conjugate gradient method for the solution of electromagnetic radiation from electrically large and small conducting bodies. *IEEE Trans. Antenna Propag.*, **AP-34,** 634–640.

Schneider, T. L., and G. L. Stephens, 1995: Theoretical aspects of modeling backscattering by cirrus ice particles at millimeter wavelength. *J. Atmos. Sci.*, **52,** 4367–4385.

Sekelky, S. M., and R. E. McIntosh, 1996: Cloud observations with a polarimetric 33-GHz and 95-GHz radar. *Meteor. Atmos. Phys.*, **59,** 123–140.

Syrett, W. J., B. A. Albrecht, and E. E. Clothiaux, 1995: Vertical structure in a midlatitude cyclone from a 94-GHz radar. *Mon. Wea. Rev.*, **123,** 3393–3407.

Ulaby, F. T., R. K. Moore, and A. K. Fung, 1981: *Microwave Remote Sensing: Active and passive.* Artech House, 456 pp.